applied sciences

MDPI

Article

Research of Kinematics and Dynamics of the Lever Lifting Mechanism Used in the Mobile Automotive Lift

Askar Seidakhmet [1,*], Amandyk Tuleshov [1], Nutpulla Jamalov [1,2], Assylbek Jomartov [1], Jacek Cieslik [3], Azizbek Abduraimov [1], Aziz Kamal [1], Madi Kaliyev [1] and Kuatbay Bissembayev [1]

[1] Joldasbekov Institute of Mechanics and Engineering, Kurmagazy Str. 29, Almaty 050010, Kazakhstan; aman_58@mail.ru (A.T.); j.nutpulla@gmail.com (N.J.); legsert@mail.ru (A.J.); zizo_waterpolo@mail.ru (A.A.); kan77705@gmail.com (A.K.); mkaliev@gmail.com (M.K.); kuat_06@mail.ru (K.B.)
[2] Faculty of Mechanical Mathematics, Al Farabi Kazakh National University, Al-Farabi Avenue 71, Almaty 050040, Kazakhstan
[3] Department of Robotics and Mechatronics, AGH University of Krakow, Mickiewicza 30, 30-059 Krakow, Poland; cieslik@agh.edu.pl
* Correspondence: seydakhmet56@gmail.com; Tel.: +7-777-257-6782

Abstract: Most of the arm lifts used in today's industry are designed and manufactured based on the scissor mechanism. Such schemes have one drawback: when the mechanism is raised, their connection points with the base and the movable platform narrow, which leads to a let-down in its stability. This article proposes a new scheme for the lifting device, which eliminates the above disadvantage of scissor schemes. In the scheme developed by the authors, the joints connecting the mechanism to the moving platform and the base are fixed, which means that the distance between the connection points does not change, leading to its stable operation. The mechanism consists of one group of links of the second class and two groups of links of the fourth class. The article focuses on the stability of an automotive lift's design when moving with a load. The article presents the results of a kinematic and kinetostatic analysis, a study of the stability of the lift and the results of studies of an experimental sample of the developed lift. The methods presented in this article allow for the design of automotive lifts with new lever mechanisms, as demonstrated by computer modeling and experiments.

Keywords: lever mechanism; automotive lift; kinetostatics; link; stability

Citation: Seidakhmet, A.; Tuleshov, A.; Jamalov, N.; Jomartov, A.; Cieslik, J.; Abduraimov, A.; Kamal, A.; Kaliyev, M.; Bissembayev, K. Research of Kinematics and Dynamics of the Lever Lifting Mechanism Used in the Mobile Automotive Lift. *Appl. Sci.* **2023**, *13*, 11361. https://doi.org/10.3390/app132011361

Academic Editor: Marco Troncossi

Received: 7 September 2023
Revised: 10 October 2023
Accepted: 13 October 2023
Published: 16 October 2023

1. Introduction

In many industrial production areas, automotive lifts are widely used at present. Among them are the construction industry, large-scale trade (malls), agro-industry, logistics of terminals and transport warehouses (airports, railway transport, road and sea transport), military equipment, etc. The Automotive Scissor Arm Lift is used for stacking, lifting or lowering, transporting and/or moving material [1].

The lever scissor mechanism is efficient in lifting loads [2–5]. Raising or lowering of the lever scissor mechanism is carried out by moving hydraulic drives or a linear actuator, which acts on the scissor mechanism and causes the vertical movement of the working platform. The design of the scissor mechanism causes the automotive lift with a scissor arm mechanism to have poor stability. When lifting the load, the distance between the attachment points of the scissor mechanism to the base and the movable platform decreases; therefore, the base of the scissor mechanism decreases (Figure 1) and, accordingly, it becomes possible to overturn the automotive lift [6,7]. There were 78 accidents while using a scissor lift between 1992 and 2003, according to the Census of Fatal Occupational Injuries (CFOI) [8]. The finite element method was used to design a scissor mechanism in [9,10]. The method of bond graphs was used to study the dynamics of a scissor mechanism in [11].

The modeling of a scissor mechanism that utilizes curvilinear and pneumatic drives to implement the curvilinear movement of a moving platform is discussed in [12–19].

(**a**) (**b**)

Figure 1. Positions of the base of the scissor mechanism (**a**) in the folded state and (**b**) in the maximum raised state.

This article considers the scheme of a new lever mechanism [20,21], where the joints of the connection of the mechanism to the movable platform and the base are fixed motionless, i.e., the distance between the connection joints does not change. The stability of this lifting mechanism scheme is improved compared to the scissor mechanism. Developing and researching a lifting lever mechanism with a fixed base is a pressing matter. The subject of this article is the study of the proposed lift.

The novelty of the research lies in the new design of the lever mechanism of the lift, where the joints of the connection of the mechanism to the movable platform and the base are fixed and motionless, which increases stability compared to the scissor mechanism; the development of methods for kinematic and kinetostatic analysis of the mechanism; the study of the stability of an automotive lift with a load on a moving platform and determination the boundaries of the stability area; the experimental measurement of stresses in mechanism links and the comparison with the results of numerical calculations.

This article has the following structure.

Section 1 provides an overview of the research methods of the scissor mechanism used in the moving platforms and the disadvantages of such a mechanism. The design of a new lever mechanism that has improved stability compared to the scissor mechanism and the methods required are discussed.

Section 2 concentrates on the design of a new lifting lever mechanism. The new lifting lever mechanism's design was examined, and it was found that it consists of two main modules. The analysis of the kinematics of the spatial mechanism was conducted based on a study of its flat scheme.

Section 3 describes the equations for finding reactions in cylindrical pairs of link connections, which were determined on the basis of general dynamic equations in the form of the d'Alembert–Lagrange equations.

Section 4 deals with the forces acting on the structure of an automotive lift. The condition for the stability of an automotive lift under the action of external forces, including

the load's gravity, has been articulated. The boundaries for the lift stability area of an automotive lift have been determined.

Section 5 describes the results of experimental studies on the determination stresses in the links of the mechanism and compares them with the results of the calculated stresses using the d'Alembert–Lagrange equations.

The conclusions that were obtained as a result of the research are presented in Section 6.

2. Materials and Methods

This section describes the derivation of kinematic equations for a new spatial lifting lever mechanism. Analysis of design of the lever mechanism allowed us to identify two main units (Figure 2): a spatial structure of seven links (4, 5, 6, 7, 8, 9, 10—black color) and four-link mechanism (0, 1, 2, 3—red color). For a flat diagram of a lever mechanism (Figure 3), vectors were introduced along the links of the mechanism, and closed vector contours were considered. Then, projection equations on the x and y axes were written for the vector equations. Graphs of changes in angular velocities and accelerations of the links were obtained by numerically solving these equations, depending on the angle of rotation of the first link.

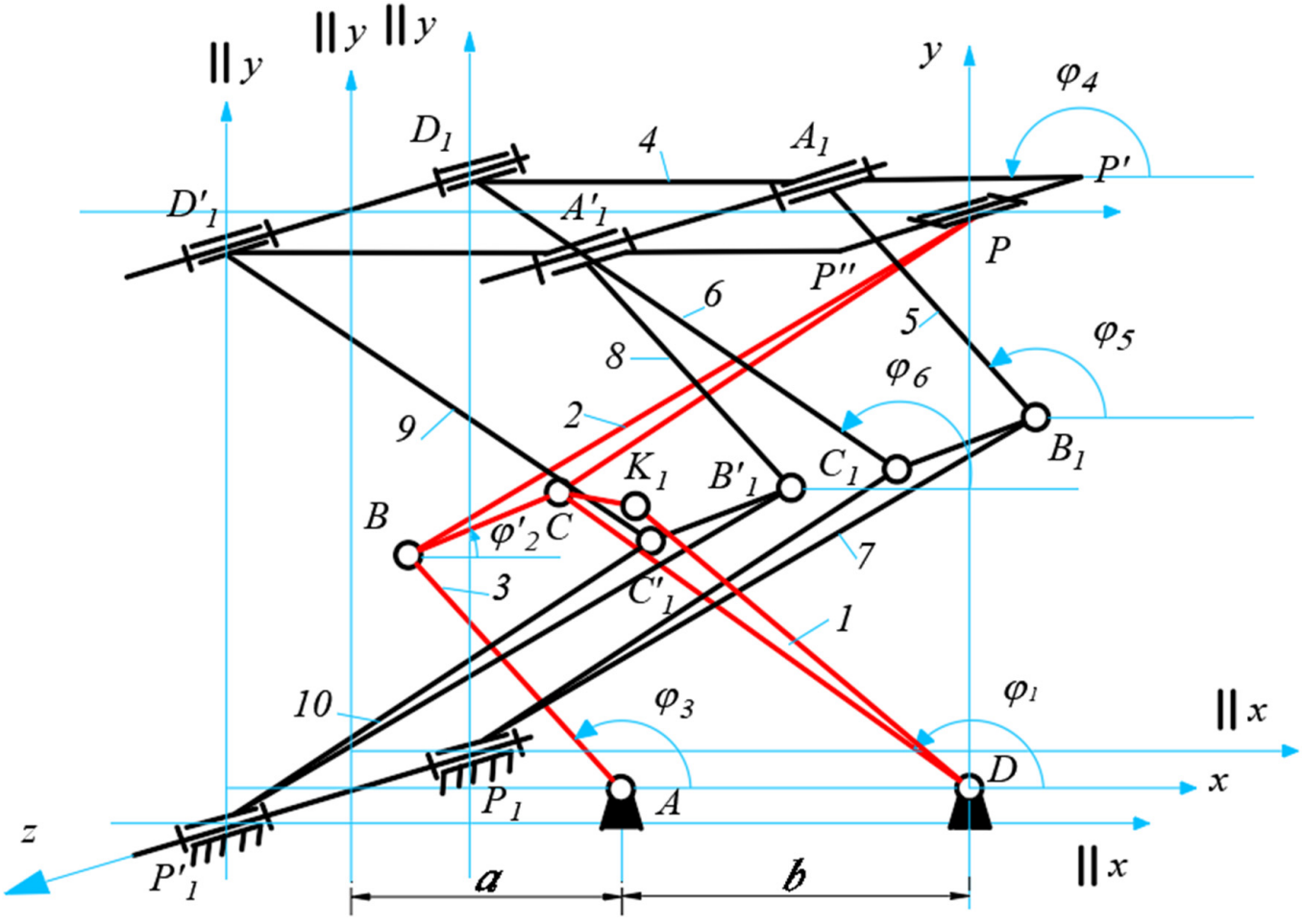

Figure 2. Spatial kinematic diagram of the new lever lifting mechanism.

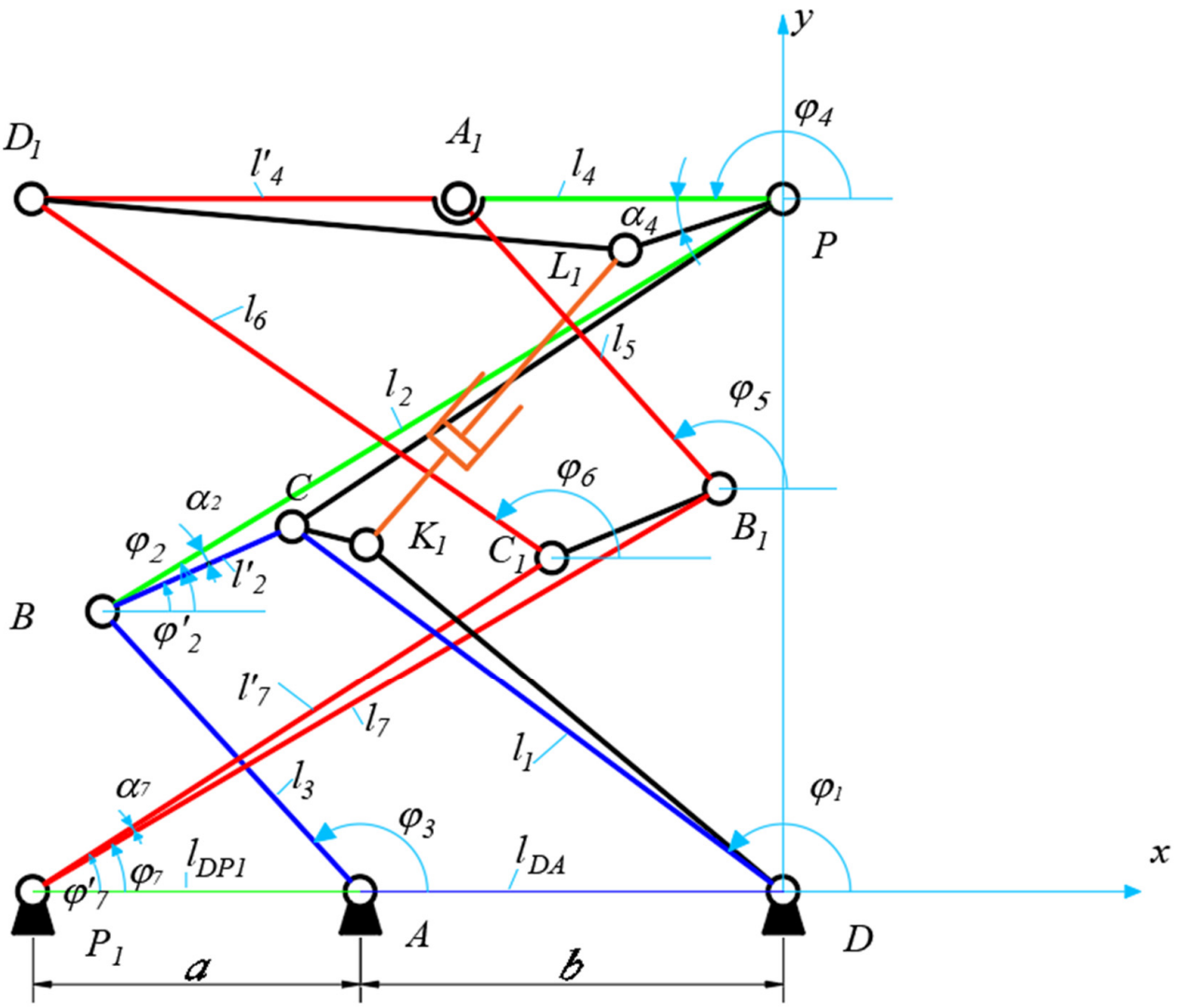

Figure 3. Flat kinematic diagram of the lever lifting mechanism.

2.1. Design of a New Lifting Lever Mechanism

The analysis of the use of the scissor mechanism in lifting mechanisms of automotive lifts revealed the need for designing a lever mechanism in which the joints of the connection of the mechanism to the movable platform and the base are fixed motionless, which has increased stability compared to the scissor mechanism.

At the Joldasbekov Institute of Mechanics and Engineering (Republic of Kazakhstan, Almaty), a lever lifting mechanism with the joints of the connection of the mechanism to the movable platform and the base, the spatial scheme of which is shown in Figure 2, was synthesized [20,21].

2.2. Kinematic Relations

This mechanism has the following relations:

(1) parallelism of the axes of rotation of the links, i.e., $D_1D\prime_1 \| A_1A\prime_1 \| C_1C\prime_1 \| B_1B\prime_1 \| P_1P\prime_1 \|$;
(2) mutual equality of the lengths of the links, i.e., $D_1A_1 = D'_1A'_1 = AD$, $D_1C_1 = D'_1C'_1 = DC$, $A_1B_1 = A'_1B'_1 = AB$, $P_1C_1 = P'_1C'_1 = CP$, $P_1B_1 = P'_1B'_1 = BP$, $C_1B_1 = C'_1B'_1 = BC$.

Thus, the kinematics of the spatial mechanism can be considered on the basis of the study of its flat scheme (Figure 3), which is a projection of the original mechanism on the Oxy plane.

The flat kinematic scheme of the lever lifting mechanism is a mechanism that consists of the following structural groups: input link (1), two-link group (2,3) and four-link group (4,5,6,7). Table 1 shows the constant geometric dimensions of the links of the lifting lever mechanism.

Table 1. The constant geometric dimensions of the links of the lifting lever mechanism.

$DC=l_1$	$BC=l_2$	$BP=l'_2$	$AB=l_3$	$PD_1=l_4$	$PA_1=l'_4$
1178.8 mm	358.49 mm	1532.72 mm	704.628 mm	1500.0 mm	648.3 mm
$C_1D_1 = l_6$	$A_1B_1 = l_5$	$P_1B_1 = l_7$	$P_1C_1 = l'_7$	$P_1A = a$	$AD = b$
1178.8 mm	704.628 mm	1532.7 mm	1171.5 mm	648.3 mm	851.7 mm

Variable geometric parameters of the lever lifting mechanism are as follows: φ_i, $i = 1, 2, 3, 4, 5, 6, 7$.

We chose the origin of coordinates at point D. The kinematic equations of the lever mechanism were written using the vector method: first, vectors were introduced along the links of the mechanism; after that, closed vector contours $DCBAD$ (blue color), $DABPA_1B_1P_1D$ (blue, green and red colors) and $P_1B_1A_1D_1C_1P_1$ (red color) (Figure 3), were considered; and finally, vector equations were written. Then the following vector equations take place:

$$\vec{l_1} + \vec{l'_2} = \vec{l_{DA}} + \vec{l_3}, \tag{1}$$

$$\vec{l_{DA}} + \vec{l_3} + \vec{l_2} + \vec{l_4} = \vec{l_{DP_1}} + \vec{l_7} + \vec{l_5} \tag{2}$$

$$\vec{l_7} + \vec{l_5} + \vec{l'_4} = \vec{l'_7} + \vec{l_6} \tag{3}$$

Note that Equation (1) shows the kinematics equations of the four-link mechanism (0,1,2,3), and Equations (2) and (3) are the kinematics equations of the adjoint four-link group (4,5,6,7).

Projecting Equations (1)–(3) onto the x, y axes, we obtain six scalar equations with eight unknowns φ_i, $i = 2, 3, 4, 5, 6, 7$ for a given φ_1:

(a) for a four-link (0,1,2,3)

$$\begin{cases} l_1 cos(\varphi_1) + l'_2 cos(\varphi'_2) = -b + l_3 cos(\varphi_3) \\ l_1 sin(\varphi_1) + l'_2 sin(\varphi'_2) = l_3 sin(\varphi_3) \end{cases}, \tag{4}$$

(b) for the group (0,2,3,4,5,7)

$$\begin{cases} -b + l_3 cos(\varphi_3) - l_2 cos(\varphi'_2 + \alpha_2) + l_4 cos(\varphi_4) = -(a+b) + l'_7 cos(-\varphi'_7 + \alpha_7) + l_5 cos(\varphi_5) \\ l_3 sin(\varphi_3) - l_2 sin(\varphi'_2 + \alpha_2) + l_4 sin(\varphi_4) = l'_7 sin(-\varphi'_7 + \alpha_7) + l_5 sin(\varphi_5) \end{cases} \tag{5}$$

(c) for the group (4,5,6,7)

$$\begin{cases} l_7 cos(-\varphi'_7 + \alpha_7) + l_5 cos(\varphi_5) + l'_4 cos(-\varphi'_4 + \alpha_4) = l'_7 cos(\varphi'_7) + l_6 cos(\varphi_6) \\ l_7 sin(-\varphi'_7 + \alpha_7) + l_5 sin(\varphi_5) + l'_4 sin(-\varphi'_4 + \alpha_4) = l'_7 sin(\varphi'_7) + l_6 sin(\varphi_6) \end{cases}, \tag{6}$$

To find the angular velocities ω_2 *and* ω_3 of links 2 and 3, we differentiate the system of Equation (4).

$$\begin{cases} \omega_1 l_1 sin(\varphi_1) + \omega_2 l'_2 sin(\varphi'_2) = \omega_3 l_3 sin(\varphi_3) \\ \omega_1 l_1 cos(\varphi_1) + \omega_2 l'_2 cos(\varphi'_2) = \omega_3 l_3 cos(\varphi_3) \end{cases}, \tag{7}$$

Resolving Equation (7) we find the angular velocities ω_2 *and* ω_3. To find the links of the angular velocities ω_4, ω_5, ω_6 *and* ω_7, we differentiate the system of Equations (5) and (6).

$$\begin{cases} -\omega_3 l_3 sin(\varphi_3) + \omega_2 l'_2 sin(\varphi'_4 + \alpha_4) - \omega_4 l_4 sin(\varphi_4) = \omega_7 l_7 sin(-\varphi'_7 + \alpha_7) - \omega_5 l_5 sin(\varphi_5) \\ \omega_3 l_3 cos(\varphi_3) - \omega_2 l'_2 cos(\varphi'_4 + \alpha_4) + \omega_4 l_4 cos(\varphi_4) = \omega_7 l_7 cos(-\varphi'_7 + \alpha_7) + \omega_5 l_5 cos(\varphi_5) \\ \omega_7 l_7 sin(-\varphi'_7 + \alpha_7) - \omega_5 l_5 sin(\varphi_5) + \omega_4 l'_4 sin(-\varphi'_4 + \alpha_4) = \omega_7 l'_7 sin(\varphi'_7) - \omega_6 l_6 sin(\varphi_6) \\ \omega_7 l_7 cos(-\varphi'_7 + \alpha_7) + \omega_5 l_5 cos(\varphi_5) + \omega_4 l'_4 cos(-\varphi'_4 + \alpha_4) = \omega_7 l'_7 cos(\varphi'_7) + \omega_6 l_6 cos(\varphi_6) \end{cases} \quad (8)$$

Resolving Equation (9), we find the angular velocities ω_4, ω_5, ω_6 *and* ω_7.

To find the angular accelerations ε_2 *and* ε_3 of links 2 and 3, we differentiate the system of Equation (7).

$$\begin{cases} \varepsilon_1 l_1 sin(\varphi_1) + \omega_1^2 l_1 cos(\varphi_1) + \varepsilon_2 l'_2 sin(\varphi_2 - \alpha_2) + \omega_2^2 l'_2 cos(\varphi_2 - \alpha_2) = \varepsilon_3 l_3 sin(\varphi_3) + \\ \omega_3^2 l_3 cos(\varphi_3) \\ \varepsilon_1 l_1 cos(\varphi_1) - \omega_1^2 l_1 sin(\varphi_1) + \varepsilon_2 l'_2 cos(\varphi_2 - \alpha_2) - \omega_2^2 l'_2 sin(\varphi_2 - \alpha_2) = \varepsilon_3 l_3 cos(\varphi_3) - \\ \omega_3^2 l_3 sin(\varphi_3) \end{cases} \quad (9)$$

Resolving Equation (9), we find the angular accelerations ε_2 *and* ε_3. To find the links of the angular accelerations ε_4, $\varepsilon_5, \varepsilon_6$ *and* ε_7, we differentiate the system of Equation (8).

$$\begin{cases} \varepsilon_3 l_3 sin(\varphi_3) + \omega_3^2 l_3 cos(\varphi_3) + \varepsilon_2 l_2 sin(\varphi_2) + \omega_2^2 l_2 cos(\varphi_2) + \varepsilon_4 l_4 sin(\varphi_4) + \omega_4^2 l_4 cos(\varphi_4) = \\ \varepsilon_7 l_7 sin(\varphi_7) + \omega_7^2 l_7 cos(\varphi_7) + \varepsilon_5 l_5 sin(\varphi_5) + \omega_5^2 l_5 cos(\varphi_5) \\ \varepsilon_3 l_3 cos(\varphi_3) - \omega_3^2 l_3 sin(\varphi_3) + \varepsilon_2 l_2 cos(\varphi_2) - \omega_2^2 l_2 sin(\varphi_2) + \varepsilon_4 l_4 cos(\varphi_4) - \omega_4^2 l_4 sin(\varphi_4) = \\ \varepsilon_7 l_7 cos(\varphi_7) - \omega_7^2 l_7 sin(\varphi_7) + \varepsilon_5 l_5 cos(\varphi_5) - \omega_5^2 l_5 sin(\varphi_5) \\ \varepsilon_7 l_7 sin(-\varphi'_7 + \alpha_7) - \omega_7^2 l_7 cos(-\varphi'_7 + \alpha_7) - \varepsilon_5 l_5 sin(\varphi_5) - \omega_5^2 l_5 cos(\varphi_5) + \varepsilon_4 l'_4 sin(-\varphi_4 + \alpha_4) \\ + \omega_4 l'_4 cos(\varphi_4) = \varepsilon_7 l'_7 sin(\varphi_7 + \alpha_7) + \omega_7^2 l'_7 cos(\varphi_7 + \alpha_7) + \varepsilon_6 l_6 sin(\varphi_6) + \omega_6^2 l_6 cos(\varphi_6) \\ \varepsilon_7 l_7 cos(-\varphi'_7 + \alpha_7) + \omega_7^2 l_7 sin(-\varphi'_7 + \alpha_7) + \varepsilon_5 l_5 cos(\varphi_5) - \omega_5^2 l_5 sin(\varphi_5) + \varepsilon_4 l'_4 cos(-\varphi_4 + \alpha_4) \\ - \omega_4^2 l'_4 sin(-\varphi_4 + \alpha_4) = \varepsilon_7 l'_7 cos(\varphi'_7) - \omega_7^2 l'_7 sin(\varphi'_7) + \varepsilon_6 l_6 cos(\varphi_6) - \omega_6^2 l_6 sin(\varphi_6) \end{cases} \quad (10)$$

Resolving Equation (10), we find the angular accelerations ε_4, $\varepsilon_5, \varepsilon_6$ *and* ε_7.

Using the Maple math software, a program for solving the problem of kinematic analysis of the lift mechanism was compiled by solving Equations (4)–(10). Figure 4 shows the graphs of the angular velocities of links 2 and 3.

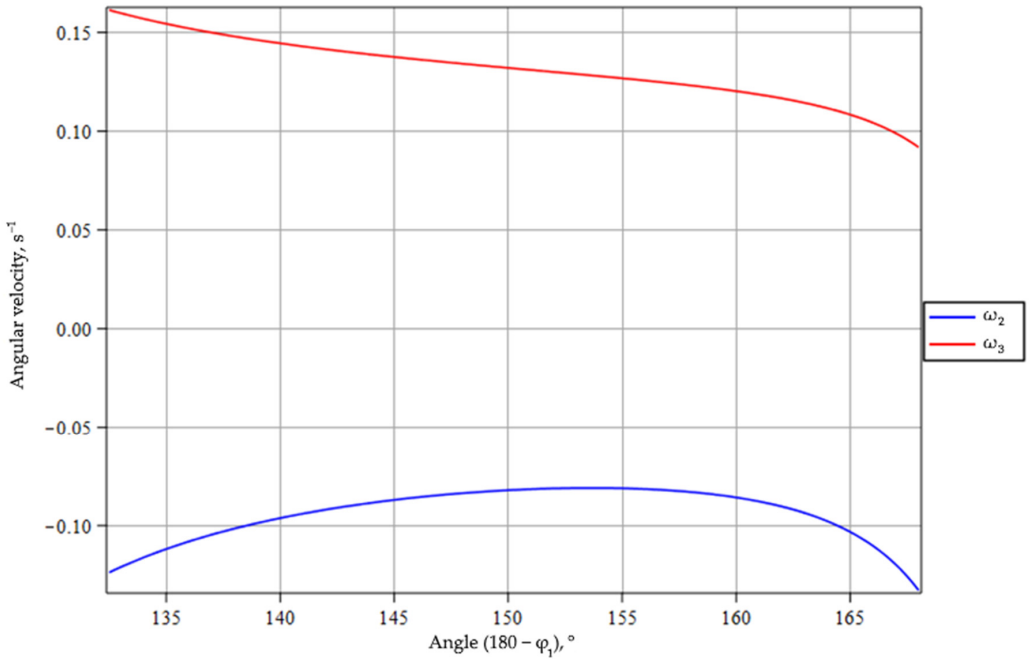

Figure 4. Graphs of the angular velocities of links 2 and 3.

Figure 5 shows the graphs of the angular velocities of links 5, 6 and 7.

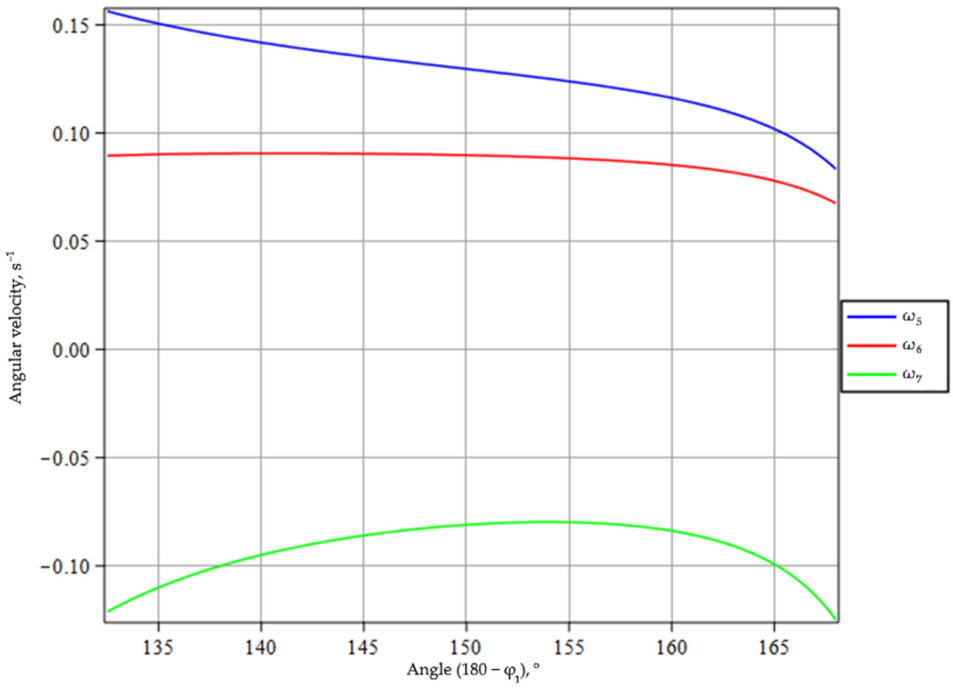

Figure 5. Graphs of the angular velocities of links 5, 6 and 7.

Figure 6 shows the graphs of the angular accelerations of links 2 and 3.

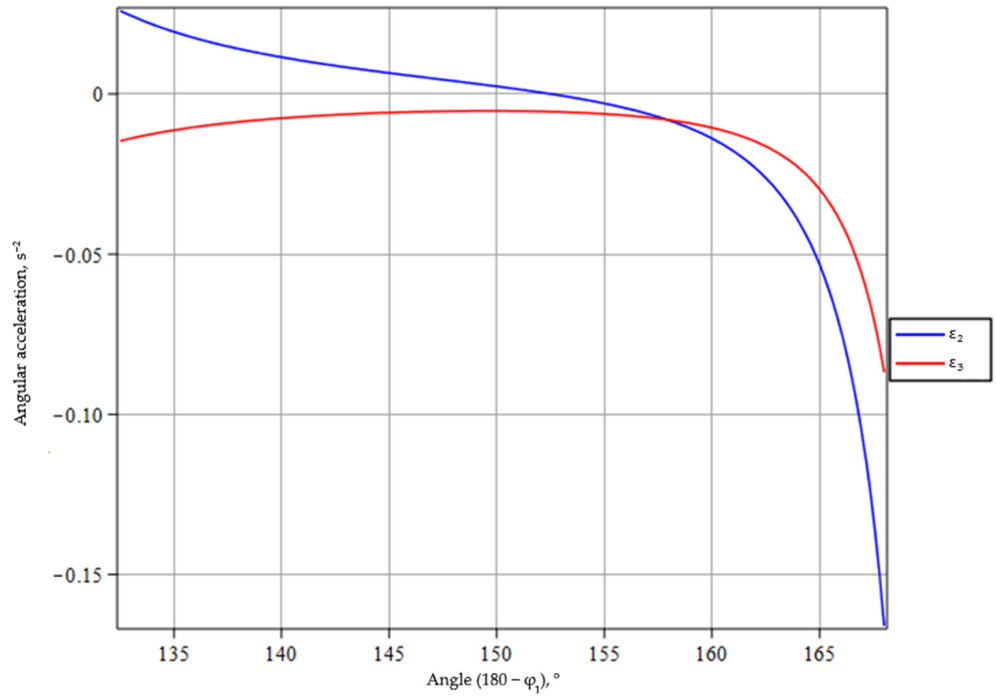

Figure 6. Graphs of angular accelerations of links 2, and 3.

Figure 7 shows the graphs of the angular accelerations of links 5, 6 and 7.

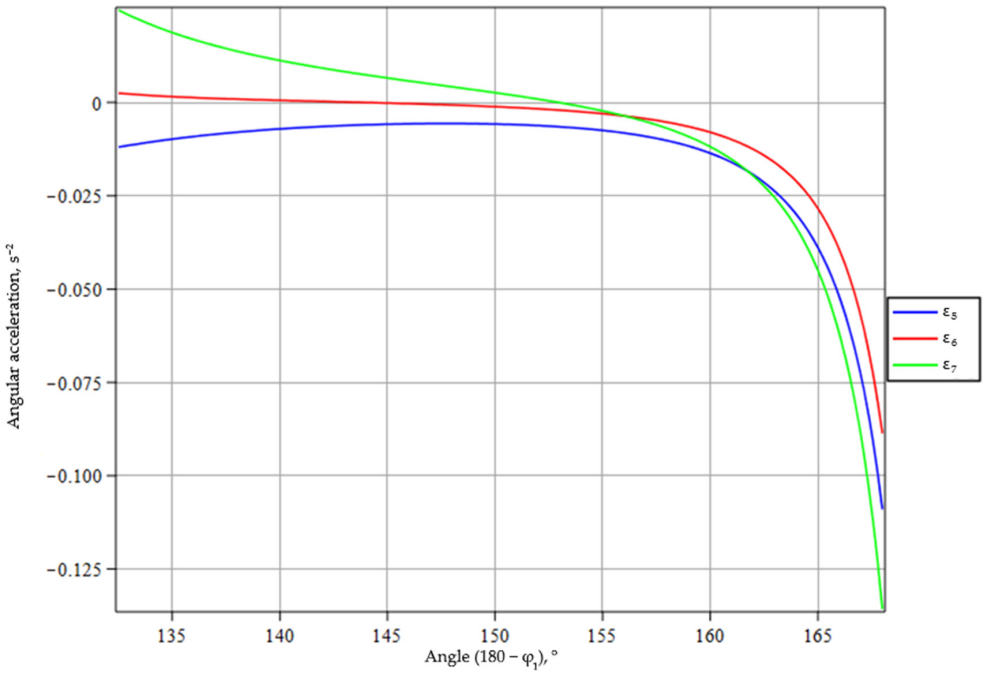

Figure 7. Graphs of angular accelerations of links 5, 6 and 7.

2.3. The Discussion of the Results from the Analysis

A separate flat kinematic chain (0,1,2,3), which was a flat four-link Chebyshev mechanism, together with flat chains (0,4,5,6,7) and (0,4,8,9,10) formed a system of three parallel circuits. The kinematic equations of this chain have an explicit analytical solution, which made it possible to write down an analytical solution for all three parallel chains connected to two parallel platforms (links). The graphs in Figures 4–7 display the changes in angular velocities and accelerations of links based on the angle of rotation of the first link. Angular velocity graphs show that the angular velocities of links 2, 5 and 6 decreased as the platform rose, and the angular velocities of links 2 and 7 had a maximum at φ_1 = 147°. Angular acceleration graphs show that the angular accelerations of links 2, 6 and 7 during the lifting of the platforms decreased in the area of positive values and increased in the area of negative values, and the angular accelerations of links 2 and 7 had a minimum of negative values at the angle of rotation φ_1 = 147° and then smoothly increased in the area of negative values. The smooth rise and fall of the lift are demonstrated by smooth and continuous changes in speeds and accelerations without any kinematic jerks.

3. Kinetostatics of the Lift Lever Mechanism

This section presents the equations in the d'Alembert–Lagrange form obtained for each link of the new lift lever mechanism. The system of equations was solved. The reaction forces in the joints and the force of balance on the driving link while lifting were determined, taking into account the forces of gravity, the inertia forces of the links and the load of 150 kg on the moving platform.

Kinetostatic equations were used to analyze and evaluate the distribution of forces to analytically determine the reactions in the joints under the influence of a load on the upper platform.

Note that link 4 performs translational motion, and links 1,2,3,5,6 and 7 perform rotational motion in planes parallel to the Oxy plane. The forces of inertia of the links are determined by the following formula:

$$\Phi_i = -m_i a_{S_i},\ i = 1, \ldots, 7, \tag{11}$$

where m_i depicts the mass of i link and a_{S_i} depicts the acceleration of the center of mass of the i link.

The moments of the forces of inertia of the rotational links are determined by the following formula:

$$\mathrm{M}_i = -J_i\varepsilon_i, \;\; i = 1, \ldots, 7, \tag{12}$$

where J_i depicts the moment of inertia of link i relative to the center of mass and S_i and ε_i depict the angular acceleration of link i.

The gravity forces of the links are determined based on the following known formulas:

$$G_i = m_i g, \;\; i = 1, \ldots, 7, \tag{13}$$

where g depicts the acceleration of the Earth.

At points K_1 and L_1, a force was applied from the pressure of the hydraulic cylinder P_{gc} and directed along the line K_1L_1. A balancing moment M_u is applied to link 1. On link 4, in the center of gravity of the link, P_h depicts the force from the action of the load on the mobile platform.

Reactions in cylindrical pairs of link connections can be determined based on the general equations of dynamics in the form of the d'Alembert–Lagrange Equation (14). It allows us to determine the reactions of all releasing connections, including those with any redundancy number.

$$\sum_{k=1}^{n} F_k \cdot \delta r_k + \sum_{k=1}^{n} \Phi_k \cdot \delta r_k = 0 \tag{14}$$

where, F_k depicts the active forces and reactions of connections, Φ_k is the inertial forces and δr_k depicts the virtual displacement.

Figure 8 shows the forces acting on the links of the lever mechanism, including inertia forces, moments of inertia forces, link gravity forces, an external force acting on the platform, balancing forces acting on link 1 and reaction forces in the joints.

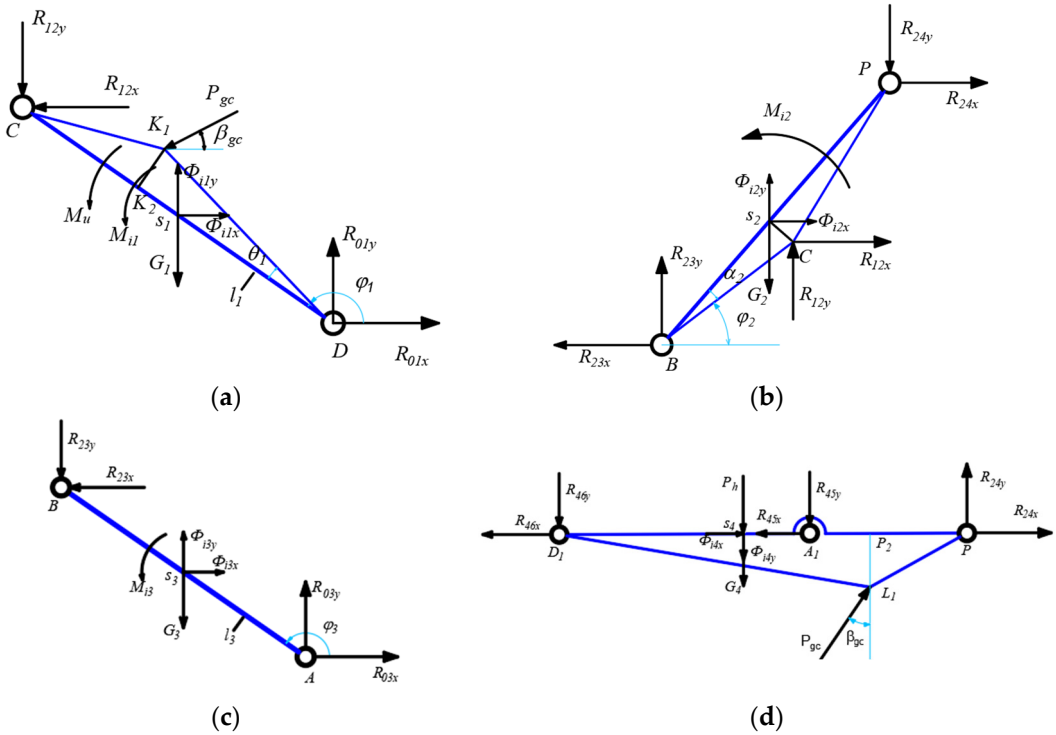

Figure 8. *Cont.*

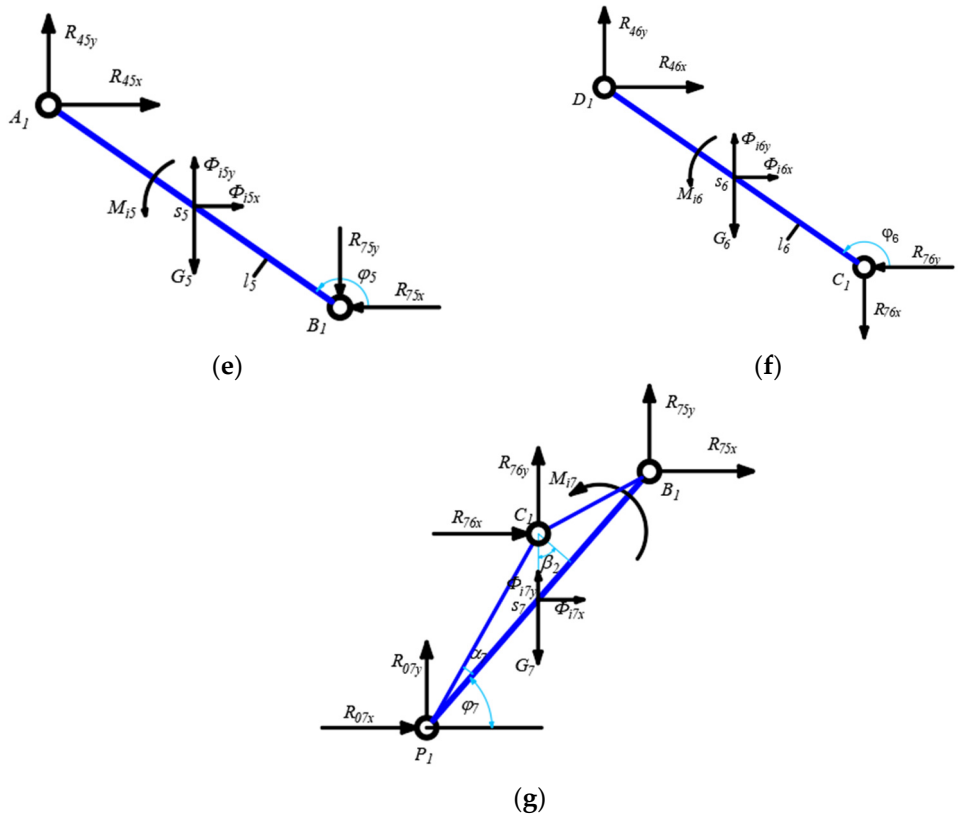

Figure 8. Forces acting on the links of the lever mechanism: (**a**)—Link 1, (**b**)—Link 2, (**c**)—Link 3, (**d**)—Link 4, (**e**)—Link 5, (**f**)—Link 6, (**g**)—Link 7.

Below are the equations of the projections of all forces acting on the links of the lever mechanism.

Link 1.

$$\begin{cases} R_{01x} - R_{12x} - m_1 a_{s1x} - P_{gc}\cos(\beta_{gc}) = 0 \\ -R_{12y} + R_{01y} - m_1 g - m_1 a_{s1y} - P_{gc}\sin(\beta_{gc}) = 0 \\ -J_{s1}\varepsilon_1 + M_u - R_{01y}\frac{l_1}{2}\cos(\varphi_1) + R_{01x}\frac{l_1}{2}\sin(\varphi_1) + R_{12x}\frac{l_1}{2}\sin(\varphi_1) - R_{12y}\frac{l_1}{2}\cos(\varphi_1) \\ -P_{gc}\cos\alpha_1\left(\frac{l_1}{2} - l_{K2C}\right) - P_{gc}\sin(\alpha_1)l_{K1K2} = 0 \end{cases} \quad (15)$$

Link 2.

$$\begin{cases} -R_{23x} + R_{24x} + R_{12x} - m_2 a_{s2x} = 0 \\ R_{23y} + R_{12y} - R_{24y} - m_2 g - m_2 a_{s2y} = 0 \\ -J_{s2}\varepsilon_2 - R_{23y}\frac{l_2}{2}\cos(\varphi_2 - \pi + \alpha_2) + R_{23x}\frac{l_2}{2}\sin(\varphi_2 - \pi + \alpha_2) \\ -R_{12x}l_{Cs2}\sin(\varphi_2 - \pi + \alpha_2 + \alpha_{Cs2}) - R_{12x}\cdot l_{Cs2}\cos(\varphi_2 - \pi + \alpha_2 + \alpha_{Cs2}) \\ -R_{24y}\cdot\frac{l_2}{2}\sin(\varphi_2 - \pi + \alpha_2) + R_{24x}\frac{l_2}{2}\sin(\varphi_2 - \pi + \alpha_2) = 0 \end{cases} \quad (16)$$

Link 3.

$$\begin{cases} R_{03x} - R_{23x} - m_3 a_{s3x} = 0 \\ R_{03y} - R_{23y} - m_3 g - m_3 a_{s3y} = 0 \\ -J_{s3}\varepsilon_3 - R_{23y}\frac{l_3}{2}\cos(\varphi_3) + R_{23x}\frac{l_3}{2}\sin(\varphi_3) - R_{03y}\frac{l_3}{2}\cos(\varphi_3) + R_{03x}\frac{l_3}{2}\sin(\varphi_3) = 0 \end{cases} \quad (17)$$

Link 4.

$$\begin{cases} -R_{46x} - R_{45x} + -R_{24x} - m_4 a_{s4x} + P_{gc}\cos\beta_{gc} = 0 \\ -R_{46y} - R_{45y} + R_{24y} - m_4 g - m_4 a_{s4y} - P_h + P_{gc} sin\beta_{gc} = 0 \\ -J_{s4}\varepsilon_4 - R_{46y}\frac{l_{DP1}}{2}\cos(\varphi_4 - \alpha_4) + R_{46x}\frac{l_{DP1}}{2}\sin(\varphi_4 - \alpha_4) - R_{24y}\frac{l_{D1P}}{2}\cos(\varphi_4) \\ +R_{24x}\frac{l_{D1P}}{2}\sin(\varphi_4) - R_{45x}\left(\frac{l_{D1P}}{2} - l_{A1P}\right)\sin(\varphi_4 - \alpha_4) + R_{45y}\left(\frac{l_{D1P}}{2} - l_{A1P}\right)\cdot \\ \cos(\varphi_4 - \alpha_4) + P_{gc}\cos(\beta_{gc}) l_{L1y} - P_{gc} sin(\beta_{gc})\left(\frac{l_{D1P}}{2} - l_{L1x}\right)\cos(\varphi_4) = 0 \end{cases} \quad (18)$$

Link 5.

$$\begin{cases} R_{45x} - R_{75x} - m_5 a_{s5x} = 0 \\ R_{45y} - R_{75y} - m_5 g - m_5 a_{s5y} = 0 \\ -J_{s5}\varepsilon_5 + R_{45y}\frac{l_5}{2} cos(\varphi_5) - R_{45x}\frac{l_5}{2} sin(\varphi_5) + R_{75y}\frac{l_5}{2} cos(\varphi_5) - R_{75x}\frac{l_5}{2} sin(\varphi_5) = 0 \end{cases} \quad (19)$$

Link 6.

$$\begin{cases} -R_{76x} + R_{46x} - m_6 a_{s6x} = 0 \\ -R_{76y} + R_{46y} - m_6 g - m_6 a_{s6y} = 0 \\ -J_{s6}\varepsilon_6 + R_{46y}\frac{l_6}{2}\cos(\varphi_6) - R_{46x}\frac{l_6}{2}\sin(\varphi_6) + R_{76y}\frac{l_6}{2} cos(\varphi_6) - R_{76x}\frac{l_6}{2} sin(\varphi_6) = 0 \end{cases} \quad (20)$$

Link 7.

$$\begin{cases} R_{07x} + R_{75x} + R_{76x} - m_7 a_{s7x} = 0 \\ R_{07y} + R_{75y} + R_{76y} - m_7 g - m_7 a_{s7y} = 0 \\ -J_{s7}\varepsilon_7 + R_{75y}\frac{l_7}{2}\cos(\varphi_7 - \alpha_7) - R_{75x}\frac{l_7}{2}\sin(\varphi_7 - \alpha_7) - R_{76x} l_{C1s7} sin(\varphi_7 - \alpha_7) \\ +R_{76y} l_{C1s7}\cos(\varphi_7 - \alpha_7) + R_{07x}\frac{l_7}{2}\sin(\varphi_7 - \alpha_7) + R_{07y}\frac{l_7}{2}\cos(\varphi_7 - \alpha_7) = 0 \end{cases} \quad (21)$$

In all equations, the following notation is adopted:

$\Phi_{ix} = -m_i a_{six}$, $\Phi_{iy} = -m_i a_{siy}$—projections of the inertia force of the i link on the x, y axes;

a_{six}, a_{siy}—acceleration projections of the center of mass of the i link on the x, y axes, $i = 1, \ldots, 7$;

R_{ij}—the reaction force in the joint from the action of the i link on the j link;

$G_i = m_i \cdot g$—the force of gravity applied at the center of mass of the i link;

P_{gc}—the force acting along the hydraulic cylinder;

P_h—the load force acting on platform 4.

Thus, a system of 21 equations with 21 unknowns was obtained. To solve this system in the Maple computer system, a program for solving the problem of kinetostatic analysis for various positions of the lever mechanism was compiled.

The Discussion of the Results from the Analysis

Equations and numerical results of the force analysis of the mechanism are obtained for a statically determinate system. The number of Equations (15)–(21) matches with the number of unknown reactions in kinematic pairs and represents a system of linear equations. This system is solved and the reactions are determined, which are further used to analyze the stress-strain state of the links in the design.

4. Analysis and Evaluation of the Stability of the Design of an Automotive Lift

This section covers an analysis and assessment of the stability of the lift mechanism with mass M_1 and a displaced load with mass M_2. An expression for the stability condition has been written down, and the boundaries of the stability area for the automotive lift have been determined. Also, an analysis of the stability of an automotive lift under specific parameters was carried out.

To analyze and evaluate the stability of the design of an automotive lift loaded with a load M_2 on the working platform, we review the forces acting on it. Figure 9 shows a

diagram of a lift with mass M_1 and a load with mass M_2 displaced relative to the ordinate of the reporting system xO_1y by the value b.

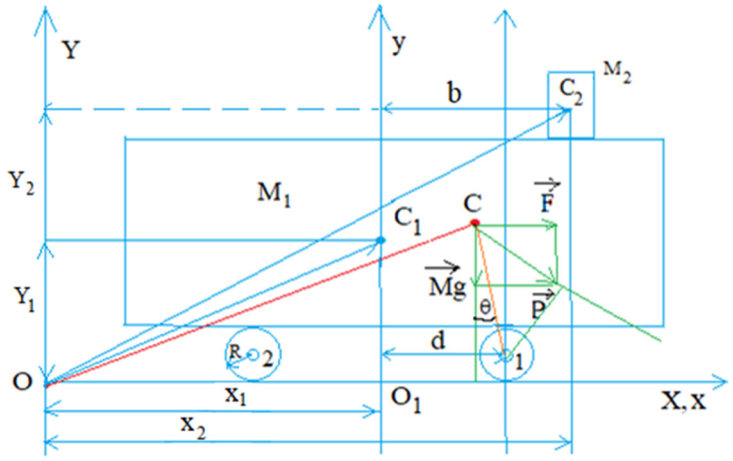

Figure 9. Scheme of an automotive lift with a mass of M_1 and a load of mass M_2.

Let us introduce two reference systems: fixed xOy and xO_1y connected with the center of mass of the lift. The coordinates of the lifter's center of mass in the fixed coordinate system are X_1, Y_1. The coordinates of the center of mass of the load in the coordinate system xO_1y are X_2, Y_2. The distance between the two wheels of the lift is $2d$; the height of the lift is H. The height of the load is h. The coordinates of the load relative to the xO_1y reporting system are b, y_2. Points C_1 and C_2 designate the centers of mass of the lift and load, respectively. Point C is the common center of gravity of the lift with the load. R is the radius of the lift wheels. M is the mass of the lift and load.

The coordinates of the common center of gravity of the lift of mass $>M_1$ with a load of mass M_2 are determined by the following formulas:

$$X_c = \frac{M_1X_1 + M_2X_2}{M_1 + M_2}, \qquad Y_c = \frac{M_1Y_1 + M_2Y_2}{M_1 + M_2} \tag{22}$$

We pass from the xOy reporting systems to xO_1y (Figure 9); then,

$$x_1 = 0, \qquad y_1 = \frac{H}{2} + 2R, \qquad x_2 = b, \qquad y_2 = \frac{h}{2} + H + 2R \tag{23}$$

Substituting (23) into Equation (22), we obtain the coordinates of the common center of gravity as follows:

$$x_c = \frac{M_2b}{M_1 + M_2}, \qquad y_c = \frac{M_1\left(\frac{H}{2} + 2R\right) + M_2\left(\frac{h}{2} + H + 2R\right)}{M_1 + M_2} \tag{24}$$

Let us transform Equation (24) to the following form:

$$x_c = \frac{m \cdot b}{1 + m}, \qquad y_c = \frac{H(1 + m) + 4R(1 + m) + h \cdot m}{2(1 + m)}, \tag{25}$$

where $m = \frac{M_2}{M_1}$.

Let us derive the stability condition for the lift. Let the lift under the action of a $\vec{F}$ force move with acceleration or deceleration $\ddot{x}$. Therefore, the following relation holds:

$$F = (M_1 + M_2)\ddot{x} = M\ddot{x} \tag{26}$$

Figure 9 shows a diagram of the forces acting on the lift. From them, one can verify that the following relation holds:

$$tg\theta = \frac{d - x_c}{y_c + R} \tag{27}$$

We write the stability condition from the condition that the vector $\vec{P}$ does not go beyond the area limited between the axles of the wheels:

$$\frac{\ddot{x}}{g} < \frac{d - x_c}{y_c - R} \tag{28}$$

where $P = \sqrt{(M\ddot{x})^2 + (Mg)^2}$.

Substituting (27) into (28) and after some transformation we obtain the following:

$$\frac{\ddot{x}}{g} < \frac{2\left[d - \frac{mb}{1+m}\right]}{H + 2R + \frac{mh}{1+m}} \tag{29}$$

Inequality (29) is the final expression of the stability condition for an automotive lift.

Using the obtained expression for the stability condition, we determine the boundaries of the stability area of the lift. The parameters of an automotive lift have the following parameters:

$$M_1 = 500 \text{ kg},\ M_2 = 150 \text{ kg},\ R = 15{\cdot}10^{-2} \text{ cm},\ H = 3 \text{ m} \tag{30}$$

Substituting $\ddot{x} = 0$ into Equation (29), we obtain the boundaries of the equilibrium stability area of the automotive lift as follows:

$$\eta = \frac{b}{d} = 1 + \frac{1}{m} \tag{31}$$

Figure 10 shows the dependencies of η on m. It follows from the resulting graph that with increasing m, i.e., with an increase in the mass of the load, the area of stability of the equilibrium of the automotive lift decreases. With $m \to \infty$; $\eta = 1$, i.e., $b = d$.

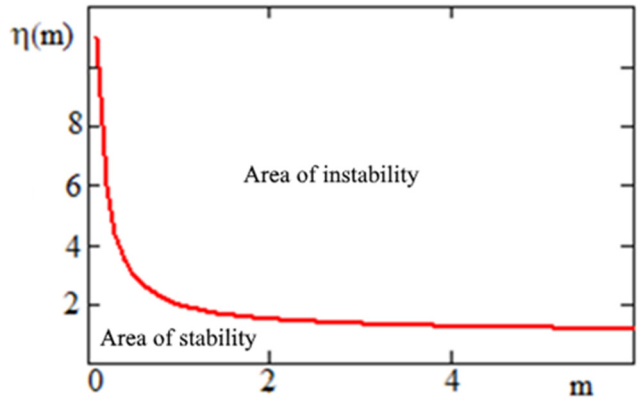

Figure 10. The area of stability of the balance of the lift with a load.

The stability conditions for an automotive lift moving from place to place and accelerating in a dimensionless form have the following form:

$$\xi = \frac{\ddot{x}}{g} < \lambda \cdot \frac{\left[1 - \frac{m}{1+m}\eta\right]}{1 + 2\frac{R}{H} + \frac{m}{1+m}\frac{h}{H}} \tag{32}$$

where $\lambda = \frac{L}{H}$, $L = 2d$—the distance between lift wheels.

Let us assume that the conditions $\frac{R}{H} \ll 1$; $\frac{h}{H} \ll 1$ are satisfied; then, Equation (32) can be written as follows:

$$\xi = \frac{\ddot{x}}{g} < \lambda \cdot \left[1 - \frac{m}{1+m}\eta\right] \tag{33}$$

It follows that $1 - \frac{m}{1+m}\eta > 0$ or $b - d < d\frac{M_1}{M_2}$, since these are the equilibrium conditions of an automotive lift.

We assume that the equilibrium of the lift is stable; therefore, the stability of an automotive lift moving from a place with acceleration depends on the height and distance between the wheels of the lift. To illustrate the stability analysis of an automotive lift, let us consider a system with the following parameters:

$$b = 1.5 \text{ m},\ d = 1 \text{ m},\ M_1 = 270 \text{ kg},\ M_2 = 90 \text{ kg},\ H = 3 \text{ m},\ L_1 = 2 \text{ m},\ L_2 = 3 \text{ m}. \tag{34}$$

Then, based on Equation (25), we obtain restrictions on the acceleration of the lift in the following form. For values $L_1 = 2$ m and $L_2 = 3$ m, the restrictions would be described by the inequalities $\frac{\ddot{x}}{g} < 0.7\frac{m}{s^2}$ and $\frac{\ddot{x}}{g} < 1\frac{m}{s^2}$, respectively. It follows that as the distance between the wheels of the lift increases, the stability area of the moving automotive lift increases, and with increasing height it decreases.

Figure 11 plots the dependence of relative accelerations ξ on the ratio λ for various η. The stability area of the lift decreases with increasing displacement of the load b relative to the lift.

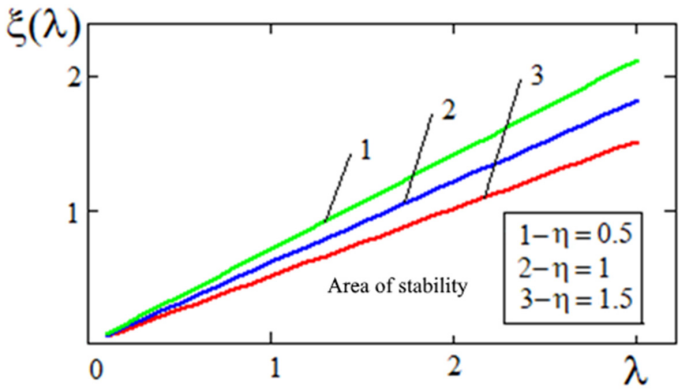

Figure 11. Graph of the dependence of relative accelerations ξ on the ratio of the distance between the wheels to the height of the lift. λ at various η.

Figure 12 shows the boundaries of the lift stability area for various values of the ratio of the mass of the load to the mass of the lift m. Based on the analysis of these graphs, it can be said that with an increase in the mass of the load, the stability area of the lift decreases.

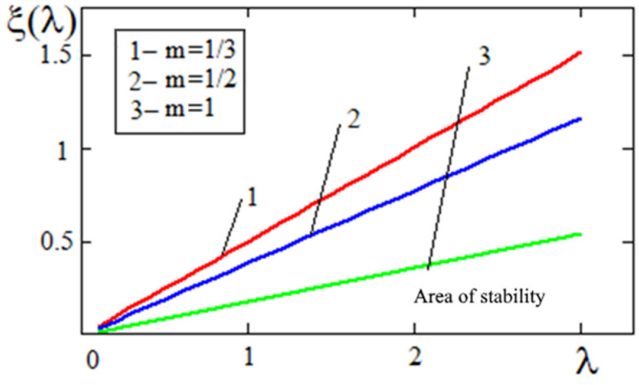

Figure 12. Graph of dependence ξ on λ at various m.

The obtained dependencies of the stability area on the parameters of the lift can be used for the optimal design of an automotive lift with a load.

5. Experimental Study of Stresses in the Links of the Lifting Mechanism

This section describes the study of stresses in the links of an experimental sample of the lever mechanism of an automotive lift with a hydraulic drive. Stress recording was carried out using a ZET 058 strain gauge system when lifting a load weighing 150 kg. The calculated stress values obtained in Section 3 were imposed on the recorded experimental graphs of stress changes over the time of lifting the load, and a comparison was made.

For the considered scheme of an automotive lift, an experimental sample of a lever lifting mechanism with a hydraulic drive was made on which stress measurements were carried out in four links, which were then compared with the calculated stress values obtained in Section 3.

Foil strain gauges were used to measure stresses in the links. Strain gauges were glued to points on the links to determine the stresses arising during the movement of the lever lifting mechanism. The strain gauges were connected to the ZET 058 strain gauge measuring system, which, together with the ZETLAB TENZO software version No. 2020.11.30 (LLC "ZETLAB", Moscow, Zelenograd, Russia), allows for collecting information from the strain gauges in real time via eight channels simultaneously.

Figure 13a shows a photograph of an experimental automotive lift; Figure 13b shows the points of sticking four strain gauges onto the links of the mechanism. Figure 14 shows the change in normal stresses at point 1 of the lift mechanism link when lifting with a load of 150 kg.

(**a**) (**b**)

Figure 13. (**a**) Photograph of an automotive lift; (**b**) points of sticking of strain gauges on the links of the lifting mechanism.

To impose the calculated curve on the experimental curve, a recalculation was made for the abscissa axis of the calculated curve depending on the angle of rotation according to the following formula:

$$\varphi_1 = \omega_1 t \tag{35}$$

where ω_1 depicts the angular speed of lifting of the first link t depicts the lifting time of a load weighing 150 kg obtained during the experiment.

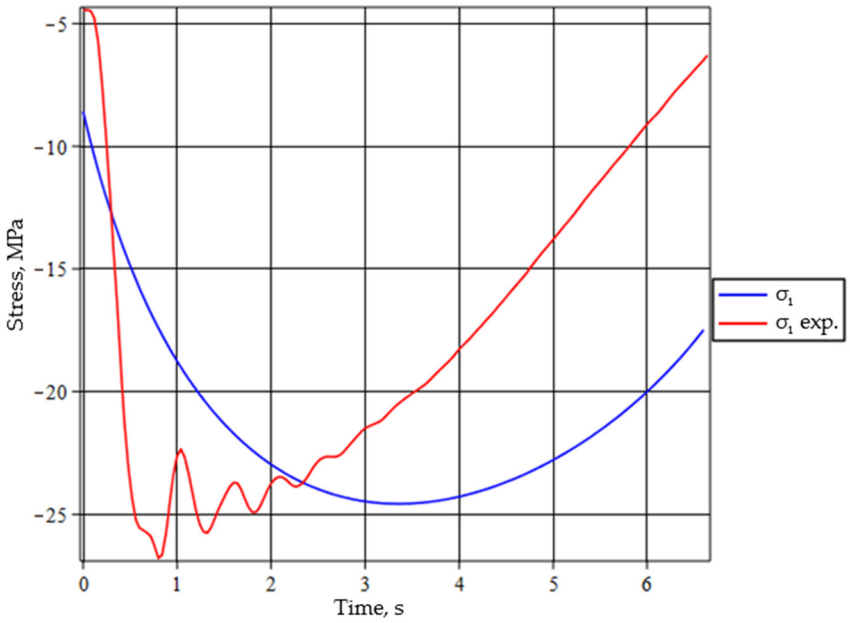

Figure 14. Calculated and experimental change in normal stresses at point 1 of the link of the lift mechanism when lifting a load weighing 150 kg.

Figure 15 shows the experimental value of the stress recorded in the middle of link 1 and the calculated value of the stress when lifting the mechanism with a load of 150 kg. The maximum stress is equal to 26.8 MPa. The experimental curve has fluctuations that arise due to the acceleration of the mechanism when lifting a load of 150 kg.

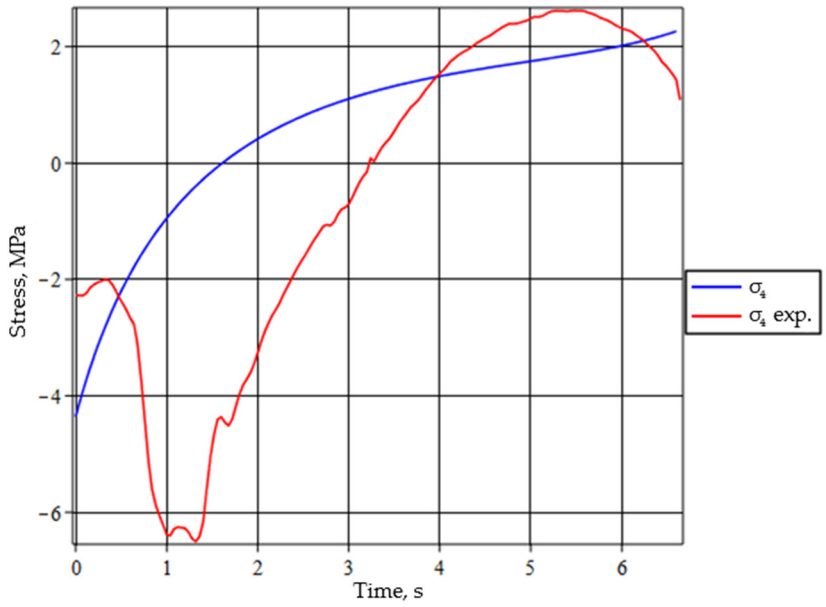

Figure 15. Calculated and experimental change in normal stresses at point 4 of the link of the lift mechanism when lifting from a load weighing 150 kg.

As can be seen from Figure 14, the experimental curve of normal stress recorded at point 4 (middle of link 7) when lifting the mechanism with a load of 150 kg has a maximum stress of −6.4 MPa and a minimum value of 1.4 MPa. The calculated curve for the normal

stress σ_4 looks like an approximately inclined line from −3.3 MPa to 1.7 MPa. The stress values in the links under a load of 150 kg are small and do not exceed 27 MPa.

As can be seen from Figures 14 and 15, the study using the d'Alembert–Lagrange equations provides an approximate description of the dynamics without taking into account oscillatory phenomena in the lift mechanism during its movement. The obtained values of stress in the links are sufficient for selecting the sections of the links of the lever mechanism.

6. Conclusions

In this article, the scheme of a new lever mechanism of the lift was considered, where the joints connecting the mechanism to the movable platform and the base are fixed. This type of lifting mechanism has increased stability compared to the scissor mechanism. Methods of kinematic analysis of the lever mechanism and kinetostatic analysis of the lever mechanism under the action of a load on a mobile platform were developed for the design of the new lever mechanism of the lift. Research on the stability of an automotive lift with a displaced load along the moving platform was carried out, and the boundaries of the stability were determined. Experimental measurements of stresses in four links were carried out and compared with the calculated stress values. The experiment showed that the scheme of the new lever mechanism of the lift is operational; stresses in the links of the mechanism under a load of 150 kg have maximum values of 27 MPa.

All of the research methods described in this article are applied only to the design of a new lift lever mechanism.

Author Contributions: Conceptualization, A.T., A.S. and K.B.; methodology, A.T., A.S. and J.C.; formal analysis, A.J., A.A., A.K. and M.K.; research, A.T. and A.S.; data processing, A.J., A.A., A.K. and M.K.; writing—preparation of the original project, N.J. and M.K.; writing—reviewing and editing, A.S., A.T., K.B. and J.C.; architectural supervision, A.T. and A.S.; project administration, A.T. and J.C.; fundraising, K.B. All authors have read and agreed to the published version of the manuscript.

Funding: The authors would like to express their sincere gratitude for the financial support provided by two grants from the Ministry of Science and Higher Education of the Republic of Kazakhstan: the Researchers Grant (Grant Number: AP09260130) to Dr. Bissembayev and the Fundamental Research Grant (Grant Number: BR20280990) to Joldasbekov IME.

Institutional Review Board Statement: Not applicable.

Informed Consent Statement: Not applicable.

Data Availability Statement: Not applicable.

Conflicts of Interest: The authors declare no conflict of interest.

References

1. Burkart, M.J.; McCann, M.; Paine, D.M. *Elevated Work Platforms and Scaffolding: Job Site Safety Manual*; McGraw-Hill: New York, NY, USA, 2004.
2. Chaudhari, P.; Maheshwari, A. Vertical Lifting System—Scissor Lift: A Review. *J. Emerg. Technol. Innov. Res.* **2020**, *7*, 233393493.
3. Liu, T.; Sun, J. Simulative calculation and optimal design of scissor lifting mechanism. In Proceedings of the 2009 Chinese Control and Decision Conference, Guilin, China, 17–19 June 2009; pp. 2079–2082.
4. Hongyu, T.; Ziyi, Z. Design and simulation based on pro/E for a hydraulic lift platform in scissors type. *Procedia Eng.* **2011**, *16*, 772–781. [CrossRef]
5. Akgün, Y.; Gantes, C.J.; Sobek, W.; Korkmaz, K.; Kalochairetis, K. A novel adaptive spatial scissor-hinge structural mechanism for convertible roofs. *Eng. Struct.* **2011**, *33*, 1365–1376. [CrossRef]
6. Guo, K.; Pan, C.Y.; Zahng, X.; Deng, H. A method of establishing and analyzing universal kinematics model based on plane scissor-like element. *Mach. Des. Res.* **2010**, *26*, 27–30.
7. Raskin, I. Stiffness and Stability of Deployable Pantographic Columns. PhD Thesis, University of Waterloo, Waterloo, ON, Canada, 1998.
8. Pan, C.S.; Hoskin, A.; McCann, M.; Lin, M.; Fearn, K.; Keane, P. Aerial lift fall injuries: A surveillance and evaluation approach for targeting prevention activities. *J. Saf. Res.* **2007**, *38*, 617–625. [CrossRef] [PubMed]
9. Hamidi, B.; Marjan, G. Design and calculation of the scissors-type elevating platforms. *Open J. Saf. Sci. Technol.* **2012**, *2*, 8–15.

10. Narasimha Murthy, P.S.K.; Vinod Prabhakara Rao, D.; Sai Vinay, C.H.; Ramesh Kumar, S.; Sai Narayan, K. Modeling and Analysis (Linear Static) on a Scissor Lift. *Int. J. Mech. Eng. Inf. Technol.* **2014**, *2*, 754–760.
11. Islam, M.T.; Yin, C.; Jian, S.; Rolland, L. Dynamic analysis of Scissor Lift mechanism through bond graph modeling. In Proceedings of the 2014 IEEE/ASME International Conference on Advanced Intelligent Mechatronics (AIM), Besacon, France, 8–11 July 2014; pp. 1393–1399.
12. Sun, Y.; Pancheri, F.; Lueth, T.C. Kinematic Modeling of Scissor-Mechanism-Based Curvilinear Actuator. In Proceedings of the IECON 2022—48th Annual Conference of the IEEE Industrial Electronics Society, Brussels, Belgium, 17–20 October 2022; pp. 1–6.
13. Yu, B.; Yang, J.; Du, R.; Zhong, Y. A Versatile Pneumatic Actuator Based on Scissor Mechanisms: Design, Modeling, and Experiments. *IEEE Robot. Autom. Lett.* **2021**, *6*, 1288–1295. [CrossRef]
14. Seidakhmet, A.Z.; Ibraev, S.M.; Drakunov, Y.M.; Tuleshov, A.K.; Abduraimov, A.E. Lift. Innovative patent for invention No. 31587, 27 September 2016.
15. Abdraimov, E.S.; Tuleshov, A.K.; Kaltaev, A.Z.; Seidakhmet, A.Z.; Abduraimov, A.E.; Gritsenko, I.S.; Noruzbaev, Z.D. Support and Lifting Device. Eurasian Patent for Invention No. 036817; Application No. 201900336, 23 December 2020.
16. Rote, D.; Kolhe, K. Optimisation in design of mechanical scissor lift. *Int. Eng. Res. J. Spec.* **2016**, *3*, 35–39.
17. Yimer, W.; Wang, Y. Design, analysis and manufacturing of double scissors lift elevated by one hydraulic cylinder. *Int. J. Eng. Res. Technol.* **2019**, *8*, 709–713.
18. Thorat, S.G.; Chiddarwar, A.R.; Prasana, S. Design and construction of hydraulic scissor lift. *Int. J. Curr. Eng. Technol.* **2017**, *7*, 32–95.
19. Ciupan, C.; Ciupan, E.; Pop, E. Algorithm for designing a hydraulic scissor lifting platform. In Proceedings of the Modern Technologies in Manufacturing (MTeM 2019), Online, 2 December 2019; Volume 299, p. 03012. [CrossRef]
20. Jomartov, A.; Tuleshov, A. Vector method for kinetostatic analysis of planar linkages. *J. Braz. Soc. Mech. Sci. Eng.* **2018**, *40*, 56. [CrossRef]
21. Jomartov, A.A.; Tuleshov, A.K.; Halicioglu, R.; Kuatova, M.Z. Simulation of the crank press dynamics by SimulationX software. *J. Math. Mech. Comput. Sci.* **2019**, *102*, 22–33. [CrossRef]